

Shape-Controlled Narrow-Gap SnTe Nanostructures: From Nanocubes to Nanorods and Nanowires

Shaojun Guo,^{*,†} Andrew F. Fidler,[†] Kai He,[‡] Dong Su,[‡] Gen Chen,[§] Qianglu Lin,[†] Jeffrey M. Pietryga,^{*,†} and Victor I. Klimov^{*,†}

[†]Center for Advanced Solar Photophysics, Chemistry Division, Los Alamos National Laboratory, Los Alamos, New Mexico 87545, United States

[‡]Center for Functional Nanomaterials, Brookhaven National Laboratory, Upton, New York 11973, United States

[§]Department of Chemical and Materials Engineering, New Mexico State University, Las Cruces, New Mexico 88003, United States

S Supporting Information

ABSTRACT: The rational design and synthesis of narrow-gap colloidal semiconductor nanocrystals (NCs) is an important step toward the next generation of solution-processable photovoltaics, photodetectors, and thermoelectric devices. SnTe NCs are particularly attractive as a Pb-free alternative to NCs of narrow-gap lead chalcogenides. Previous synthetic efforts on SnTe NCs have focused on spherical nanoparticles. Here we report new strategies for synthesis of SnTe NCs with shapes tunable from highly monodisperse nanocubes, to nanorods (NRs) with variable aspect ratios, and finally to long, straight nanowires (NWs). Reaction at high temperature quickly forms thermodynamically favored nanocubes, but low temperatures lead to elongated particles. Transmission electron microscopy studies of reaction products at various stages of the synthesis reveal that the growth and shape-focusing of monodisperse SnTe nanocubes likely involves interparticle ripening, while directional growth of NRs and NWs may be initiated by particle dimerization via oriented attachment.

Narrow-gap colloidal semiconductor nanocrystals (NCs) are of considerable interest for applications in solution-processed solar cells,¹ photodetectors,² light-emitting diodes,³ and thermoelectric devices.⁴ Among others, PbE (E = S, Se, and Te) NCs have been widely examined for practical solution-processed devices,⁵ including those utilizing carrier multiplication,⁶ whereby a single absorbed photon produces multiple excitons.⁷ Despite promising performance in various applications, the high toxicity of lead hinders widespread use of these materials in real-life technologies. Widely studied for their promising thermoelectric properties,⁸ the tin chalcogenides SnSe and SnTe are narrow-gap semiconductors that may serve as Pb-free alternatives to Pb-chalcogenides for many of the applications of interest. Similar to PbTe, SnTe possesses a rock-salt crystal structure (Figure 1a) and a very narrow (0.18 eV) direct band gap formed by four-fold degenerate conduction and valence band minima at the L-points of the Brillouin zone (Figure 1b).⁹ Also as in PbTe, carrier effective masses in SnTe are small and highly anisotropic, and the transverse mass (L–W direction of the Brillouin zone; m_t) for both electrons and holes is significantly

smaller than the longitudinal one (Γ –L direction; m_l) (Figure 1b). Because of very small carrier masses (the reduced electron/hole mass $m_{eh} \approx 0.025m_0$,¹⁰ with m_0 the free electron mass) and strong dielectric screening (the high-frequency dielectric constant $\epsilon_\infty \approx 45$), the exciton Bohr radius in SnTe is 95 nm. This is significantly larger than in any of the Pb-chalcogenides, suggesting that even fairly big particles should be influenced by effects of quantum confinement.

Earlier synthetic efforts have produced highly monodisperse spherical SnTe NCs with tunable sizes.¹¹ However, previous studies of the related Pb-chalcogenides suggested enhanced performance in devices can be achieved through shape control, such as elongation to produce nanorods (NRs) and nanowires (NWs).¹² Because of the highly symmetrical crystal structure, synthesis of elongated Pb-chalcogenide nanostructures proved quite challenging relative to that of related CdSe nanostructures,¹³ requiring use of a unique phenomenon called oriented attachment.¹⁴ Recent attempts toward SnTe NRs produced irregularly shaped elongated structures,^{15,16} with limited control of either particle size or shape within highly heterogeneous reaction product mixtures. Here, we report a new route for the synthesis of highly monodisperse shape-controlled SnTe nanostructures with a variety of morphologies tunable from nanocubes, to NRs of variable aspect ratio, and finally to long, smooth-walled NWs. High reaction temperatures lead to the formation of the thermodynamically favored cubic shape, resulting in monodisperse SnTe nanocubes with {100} faces (Scheme 1a). On the other hand, the use of lower temperatures and the presence of a reducing species promote a growth regime that favors the formation of elongated NRs. By separately controlling the injection and reaction temperatures as well as the reaction time, the aspect ratio of the NRs can be tuned from ~1.5 to >100 (defined as the ratio of the length and the width)—all the way to the regime of one-dimensional (1D) NWs (Scheme 1b). Reaction-time-dependent morphology changes revealed by transmission electron microscopy (TEM) suggest the growth of SnTe NRs may be initiated by the formation of particle dimers, which support predominantly unidirectional growth.

To synthesize cube-shaped SnTe NCs, we react SnI_2 and trioctylphosphine telluride (TOPTe) in a mixture of oleylamine

Received: September 8, 2015

Published: November 6, 2015

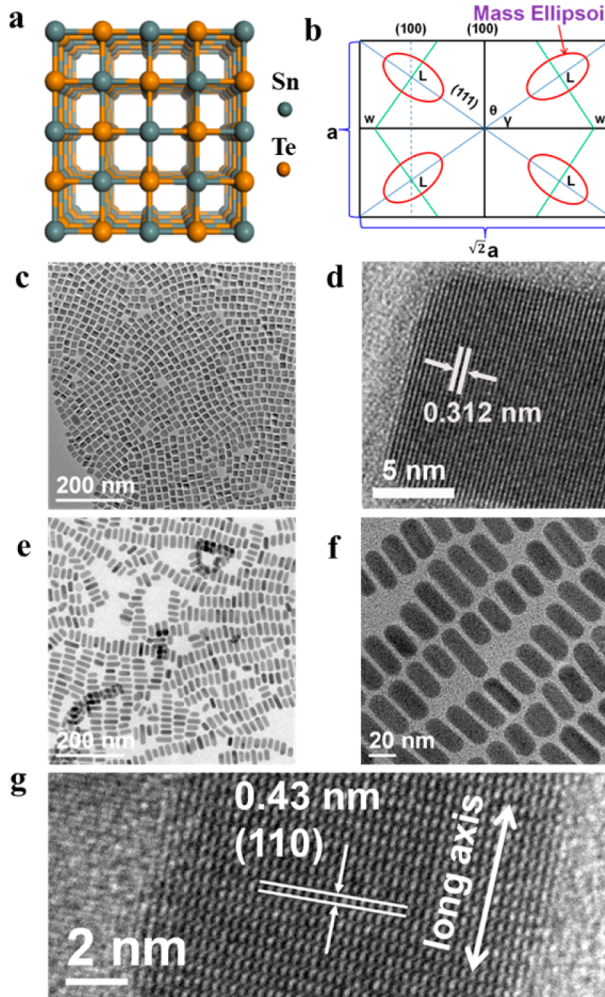


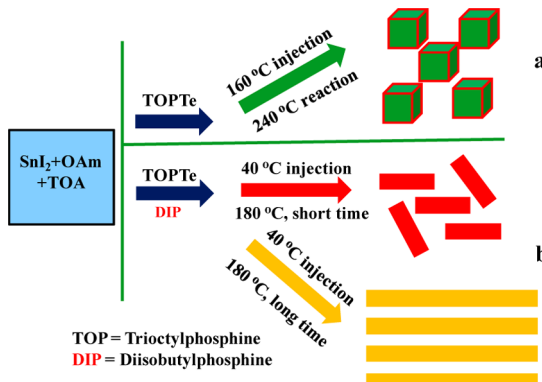
Figure 1. (a) Crystal structure and (b) two-dimensional “slice” of the Brillouin zone of rock-salt SnTe. (c,e,f) TEM and (d,g) HRTEM images of (c,d) SnTe nanocubes and (e–g) SnTe NRs.

(OAm) and trioctylamine (TOA). In a typical synthesis, 1 mmol of SnI_2 was added to 5 mL of OAm and 5 mL of TOA, and heated to 100 °C for 30 min under vacuum. The temperature was then raised to 160 °C under nitrogen, and 0.5 mL of 2 M TOPTe was injected. Following the injection, the temperature was further increased to 240 °C, and the reaction was continued for varied periods of time. The resulting SnTe NCs were isolated and purified by precipitation using a nonpolar solvent/acetonitrile mixture. The purified particles were readily dispersed in chloroform, tetrachloroethylene, or 1:1 hexane:toluene to yield a black colloidal solution (see Figure S1).

According to TEM studies, this synthesis results in monodisperse cubic SnTe NCs. Figure 1c,d shows typical TEM and HRTEM images of the SnTe nanocubes produced after 10 min of reaction at 240 °C. The mean length of the nanocube side is 16 nm, and the standard deviation is 7–8%. HRTEM images show the nanocubes are single crystalline (Figure 1d) and the lattice period is 0.312 nm, corresponding to the (200) lattice planes of bulk rock-salt α -SnTe, consistent with previous spherical SnTe NCs.¹¹ We further observe alignment of the nanocube facets with the lattice fringes, indicating they are parallel to the {100} planes.

The evolution of SnTe NC morphology during the reaction shows interesting time-dependent trends. At early times, imperfect SnTe nanocubes are observed along with some

Scheme 1. Controlled Syntheses of SnTe Nanocubes (a) and Nanorods (b) with Different Aspect Ratios



quasi-spherical nanoparticles (Figure S2a–c). Continuing growth at 240 °C for 10 min improves both size and shape uniformity and results predominantly in monodisperse 16 nm nanocubes (Figures S2d–f and S3). The cubic shape of the NCs reflects the dominance of the underlying rock-salt structure in defining the particle morphology and is consistent with similar shapes observed for large PbSe¹⁷ and PbTe NCs.¹⁸ At longer times (up to 30 min), shape uniformity worsens again as fairly long NRs begin to emerge (Figure S4). A further increase in the reaction time results in the formation of very large particles (dimensions of hundreds of nanometers) of primarily rectangular shape (Figure S5). These studies indicate that the optimal growth time for obtaining well-defined, monodisperse SnTe nanocubes is 10–20 min. This suggests an interparticle ripening process, driven by an energetic preference for flat, well-defined, and well-passivated (100) faces, to give monodisperse, cubic SnTe NCs, although instances of particle “dimerization” (see NR discussion below) can form some elongated particles.

To synthesize SnTe NRs with tunable aspect ratios, we have developed the following protocol. In a typical reaction, after the initial 30 min of reaction at 100 °C, the reaction mixture is cooled to 40 °C, followed by injection of 0.5 mL of 2 M TOPTe containing ~0.05% of diisobutylphosphine (DIP). After heating to 180 °C, the reaction is continued for different times to obtain varied aspect ratios. Figure 1e–g shows the TEM and HRTEM images of single-crystalline SnTe NRs prepared at 180 °C and growth time $t_r = 10$ min. These NRs have diameter 16 ± 4 nm and aspect ratio $\sim 2\text{--}3$. In contrast to highly irregular elongated structures reported previously,¹⁵ our synthesis does not produce branched or irregular structures, and instead results in very smooth sidewalls and a highly uniform width along the entire length of the NR. The HRTEM images reveal lattice fringes with a periodic spacing of 0.43 nm along the long axis of the NR, corresponding to the (110) planes of cubic SnTe. This confirms the rock-salt α -phase is preserved and elongation occurs along the [110] direction (Figure 1g). By progressively increasing the reaction time, we can produce nanostructures with aspect ratio varying from 1.5 to >100 nm (Figure 2a–f and Table S1). Since the larger of these values is much greater than the Bohr exciton radius in SnTe, the demonstrated size tunability covers the entire range of dimensions, from quasi-1D NRs to true-1D NWs.

We find that the NR width can be controlled by the injection temperature. By varying T_{inj} from 40 to 90 and then 120 °C, we generate NRs with widths of 15, 20, and 23 nm, respectively (Figure 2g,h). Interestingly, for a fixed reaction temperature T_r , a considerable increase in the length of the nanostructures occurs

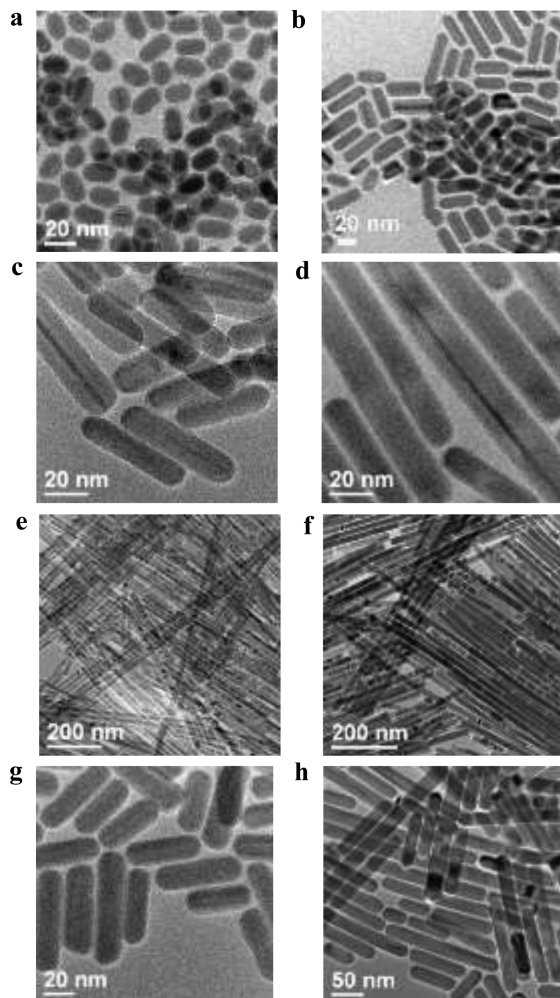


Figure 2. TEM images of SnTe NRs with different aspect ratios, prepared under different conditions. (a–f) $T_{\text{inj}} = 40^\circ\text{C}$, $T_r = 180^\circ\text{C}$, and $t_r = 0$ (a), 0.5 (b), 1 (c), 4 (d), 8 (e), and 24 h (f). (g) $T_{\text{inj}} = 90^\circ\text{C}$, $T_r = 180^\circ\text{C}$, $t_r = 3$ h. (h) $T_{\text{inj}} = 120^\circ\text{C}$, $T_r = 180^\circ\text{C}$, $t_r = 4$ h.

without significant change in their width, consistent with a mechanism in which more symmetric particles (quasi-spherical) form at early times after injection with size depending on T_{inj} . This is followed by the initial step of oriented attachment preferentially at the relatively high energy (110) facets, creating elongated “dimers”, similar to a process previously observed in colloidal SnO_2 nanoparticles.¹⁹ Under growth conditions (when precursors are still present) the difference in relative surface energy between the nominally (110) but highly curved tips and the flat side walls of the NRs favors directional growth. Careful temperature-dependent studies of particle shapes at the earliest stages of NR growth provide further evidence for this process (Figure S6), giving a significant fraction of particles with aspect ratios ~ 2 before formation of longer NRs. Importantly, we found that, in the synthesis of SnTe NRs, a small amount of DIP (while not strictly required for NR formation; see Figures S4 and S7a) is the key to obtaining a homogeneous ensemble of well-defined nanostructures without side products of other shapes: adding 0.05–0.1% of DIP to TOPTe results in well-defined SnTe NRs (Figures 1e–g and S7b), suggesting that DIP, known to be a reducing species that enhances the reactivity of precursors in Pb-chalcogenide NC synthesis,²⁰ leads to a fast growth regime

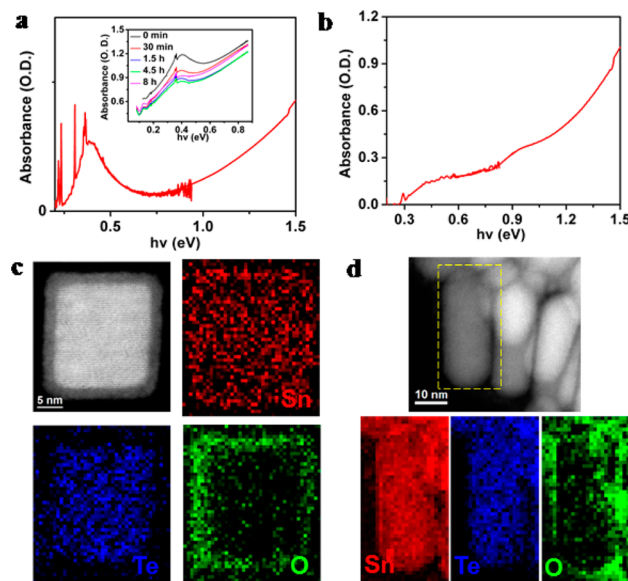


Figure 3. Optical absorption spectra of SnTe (a) nanocubes and NRs (b) dispersed in TCE. The inset of (a) shows the evolution of optical absorption spectra of SnTe nanocubes deposited on a sodium chloride disk and heated in air at 100°C for different times. STEM-EELS elemental mapping of oxidized SnTe (c) nanocubes and NRs (d).

favoring elongation of initially formed dimers over symmetrical growth.

The crystal structure and chemical composition of the nanocubes and NRs are further characterized by powder X-ray diffraction (Figure S8). Several obvious diffraction peaks can be indexed to the expected planes of the cubic rock-salt crystal structure of SnTe (space group $Fm\bar{3}m$; JCPDS no. 65-0322). No other diffraction peaks are seen, indicating the sample is highly uniform and does not evince the type of shape-dependent polymorphism observed in SnS nanostructures.²¹

To evaluate the composition of our NC samples, we conduct energy-dispersive X-ray studies of both nanocubes and NRs (Figure S9). These measurements reveal that, in contrast to typically Sn-deficient bulk material, the SnTe NCs are Sn-rich, with average Sn:Te ratios of 1.13:1 and 1.21:1 for nanocubes and NRs, respectively. This imbalance in stoichiometry in favor of a metal has been previously observed for Pb-chalcogenide NCs and explained by the presence of excess cation on the NC surfaces.²²

The absorption spectra of SnTe nanocubes dispersed in tetrachloroethylene (Figure 3a) exhibit, in addition to sharp ligand-related peaks, a pronounced feature at 385 meV, up-shifted from the bulk SnTe band gap by 205 meV. A previous report attributed this to a quantum-confined exciton transition.¹¹ Within an effective mass approximation, the confinement-induced increase in the energy gap of cubic NCs with side d can be estimated from $\Delta E_g = 3\pi^2 \hbar^2 / 2m_{\text{eh}} d^2$. Using $m_{\text{eh}} = 0.025m_0$,¹⁰ we obtain $\Delta E_g \approx 200$ meV for the 16 nm NCs. This value is remarkably close to one obtained from the blueshift of the measured absorption peak, suggesting it could correspond to the lowest energy optical transition in SnTe NCs. However, at present we cannot exclude alternative explanations of this feature, such as a predicted plasmon resonance²³ arising from self-doping.²⁴ The absorption spectrum of the NRs of average length 36 nm and width 16 nm exhibits an absorption onset at ~ 0.3 eV (Figure 3b) but does not display any prominent peaks. If this absorption indeed arises from excitonic transitions, the lack

of a distinct band-edge feature may be due to the additional inhomogeneous broadening originating from non-uniformity of the NR lengths, which is higher than the dispersity of the NR widths. Because length in these NRs is still significantly smaller than the exciton Bohr radius in SnTe, length dispersity can still contribute to the overall distribution of confinement energy in the ensemble, blurring absorption features.

To evaluate the stability of NCs under ambient atmosphere, we heat SnTe nanocubes at 100 °C in air and monitor the position of the band-edge absorption peak as a function of time (Figure 3a, inset). The absorption peak slightly decreases in intensity during the first 30 min of heating and then stabilizes, indicating an initially formed outer SnO_x layer protects the interior of the SnTe NCs from being further oxidized. This is verified by scanning TEM (STEM)–electron energy-loss spectroscopy (EELS) mapping of SnTe nanocubes and NRs (Figure 3c,d). STEM-EELS mapping reveals uniform Sn and Te distributions across the NCs and NRs interior, while the outer layer does not contain Te but instead shows the presence of O. These data indicate the SnO_x shell of ~2 nm can protect the SnTe NCs and NRs from being further oxidized, making SnTe/ SnO_x stable in the air even at high temperatures.

To summarize, we demonstrate the solution-based synthesis of monodisperse SnTe cubic NCs, elongated NRs with controlled aspect ratio, and long, straight NWs. High-temperature growth (240 °C) results in monodisperse SnTe nanocubes, whereas a lower-temperature synthesis (180 °C) produces SnTe NRs with aspect ratio tunable from 1.5 to >100 (the NW regime) by simply controlling the reaction time for a fixed reaction temperature. The NR width, on the other hand, can be controlled by the injection temperature. TEM data reveal that the formation of SnTe nanocubes relies on interparticle ripening, while dimerization via oriented attachment plays a key role in the formation of SnTe NRs. We anticipate that these relatively simple syntheses of shape-/size-controlled, Pb-free narrow-gap nanostructures will facilitate applications of colloidal IR-active nanomaterials in real-life technologies.

ASSOCIATED CONTENT

Supporting Information

The Supporting Information is available free of charge on the ACS Publications website at DOI: [10.1021/jacs.Sb09490](https://doi.org/10.1021/jacs.Sb09490).

Experimental details, data and TEM images ([PDF](#))

AUTHOR INFORMATION

Corresponding Authors

*squo@lanl.gov
*pietryga@lanl.gov
*klimov@lanl.gov

Notes

The authors declare no competing financial interest.

ACKNOWLEDGMENTS

This work was supported by the Center for Advanced Solar Photophysics (CASP), an Energy Frontier Research Center funded by the U.S. Department of Energy (DOE), Office of Science, Basic Energy Sciences. S.G. is a CASP member supported by a LANL Oppenheimer Distinguished Postdoctoral Fellowship. A.F.F. is a CASP member supported by a LANL Director's Postdoctoral Fellowship. TEM work was carried out in part at the Center for Functional Nanomaterials, Brookhaven

National Laboratory, which is supported by the DOE, Office of Basic Energy Sciences, under Contract No. DESC0012704.

REFERENCES

- (1) Beard, M. C.; Luther, J. M.; Nozik, A. J. *Nat. Nanotech.* **2014**, *9*, 951.
- (2) Konstantatos, G.; Sargent, E. H. *Nat. Nanotech.* **2010**, *5*, 391.
- (3) Steckel, J. S.; Coe-Sullivan, S.; Bulović, V.; Bawendi, M. G. *Adv. Mater.* **2003**, *15*, 1862. Konstantatos, G.; Huang, C.; Levina, L.; Lu, Z.; Sargent, E. H. *Adv. Funct. Mater.* **2005**, *15*, 1865. Sun, L.; Choi, J. J.; Stachnik, D.; Bartnik, A. C.; Hyun, B.-R.; Malliaras, G. G.; Hanrath, T.; Wise, F. W. *Nat. Nanotech.* **2012**, *7*, 369.
- (4) Tan, G.; Zhao, L.-D.; Shi, F.; Doak, J. W.; Lo, S.-H.; Sun, H.; Wolverton, C.; Dravid, V. P.; Uher, C.; Kanatzidis, M. G. *J. Am. Chem. Soc.* **2014**, *136*, 7006. Korkosz, R. J.; Chasapis, T. C.; et al. *J. Am. Chem. Soc.* **2014**, *136*, 3225.
- (5) Girard, S. N.; He, J.; Zhou, X.; Shoemaker, D.; Jaworski, C. M.; Uher, C.; Dravid, V. P.; Heremans, J. P.; Kanatzidis, M. G. *J. Am. Chem. Soc.* **2011**, *133*, 16588. Luther, J. M.; Gao, J.; Lloyd, M. T.; Semonin, O. E.; Beard, M. C.; Nozik, A. J. *Adv. Mater.* **2010**, *22*, 3704. Chuang, C.-H. M.; Brown, P. R.; Bulović, V.; Bawendi, M. G. *Nat. Mater.* **2014**, *13*, 796. Oh, S. J.; Uswachoke, C.; Zhao, T.; Choi, J.-H.; Diroll, B.-J. T.; Murray, C. B.; Kagan, C. R. *ACS Nano* **2015**, *9*, 7536.
- (6) Sukhovatkin, V.; Hinds, S.; Brzozowski, L.; Sargent, E. H. *Science* **2009**, *324*, 1542. Semonin, O. E.; Luther, J. M.; Choi, S.; Chen, H.-Y.; Gao, J.; Nozik, A. J.; Beard, M. C. *Science* **2011**, *334*, 1530. Sambur, J. B.; Novet, T. B.; Parkinson, A. *Science* **2010**, *330*, 63.
- (7) Padilha, L. A.; Stewart, J. T.; Sandberg, R. L.; Bae, W. K.; Koh, W.-K.; Pietryga, J. M.; Klimov, V. I. *Acc. Chem. Res.* **2013**, *46*, 1261. Schaller, R. D.; Klimov, V. I. *Phys. Rev. Lett.* **2004**, *92*, 186601.
- (8) Zhao, L.-D.; Lo, S.-H.; Zhang, Y.; Sun, H.; Tan, G.; Uher, C.; Wolverton, C.; Dravid, V. P.; Kanatzidis, M. G. *Nature* **2014**, *508*, 373.
- (9) Littlewood, P. B.; et al. *Phys. Rev. Lett.* **2010**, *105*, 086404.
- (10) Chen, X.; Parker, D.; Singh, D. *J. Sci. Rep.* **2013**, *3*, 3168. Volkov, B. A.; Pankratov, O. A.; Sazonov, A. V. *Zh. Eksp. Teor. Fiz.* **1983**, *85*, 1395.
- (11) Kovalenko, M. V.; Heiss, W.; Shevchenko, E. V.; Lee, J.-S.; Schwinghammer, H.; Alivisatos, A. P.; Talapin, D. V. *J. Am. Chem. Soc.* **2007**, *129*, 11354.
- (12) Bartnik, A. C.; Efros, A. L.; Koh, W.-K.; Murray, C. B.; Wise, F. W. *Phys. Rev. B* **2010**, *82*, 195313. Padilha, L. A.; Stewart, J. T.; Sandberg, R. L.; Bae, W. K.; Koh, W.-K.; Pietryga, J. M.; Klimov, V. I. *Nano Lett.* **2013**, *13*, 1092.
- (13) Peng, X.; Manna, L.; Yang, W.; Wickham, J.; Scher, E.; Kadavanich, A.; Alivisatos, A. P. *Nature* **2000**, *404*, 59.
- (14) Cho, K.-S.; Talapin, D. V.; Gaschler, W.; Murray, C. B. *J. Am. Chem. Soc.* **2005**, *127*, 7140. Koh, W.-K.; Bartnik, A. C.; Wise, F. W.; Murray, C. B. *J. Am. Chem. Soc.* **2010**, *132*, 3909.
- (15) Ning, J.; Men, K.; Xiao, G.; Zou, B.; Wang, L.; Dai, Q.; Liu, B.; Zou, G. *CrystEngComm* **2010**, *12*, 4275.
- (16) Jin, H. D.; Chang, C.-H. *J. Mater. Chem.* **2011**, *21*, 12218.
- (17) Pietryga, J. M.; Schaller, R. D.; Werder, D. J.; Stewart, M. H.; Klimov, V. I.; Hollingsworth, J. A. *J. Am. Chem. Soc.* **2004**, *126*, 11752.
- (18) Murphy, J. E.; Beard, M. C.; Norman, A. G.; Ahrenkiel, S. P.; Johnson, J. C.; Yu, P.; Mićić, O. I.; Ellingson, R. J.; Nozik, A. J. *J. Am. Chem. Soc.* **2006**, *128*, 3241.
- (19) Leite, E. R.; Giraldi, T. R.; Pontes, F. M.; Longo, E.; Beltrán, A.; Andrés, J. *Appl. Phys. Lett.* **2003**, *83*, 1566.
- (20) Steckel, J. S.; Yen, B. K. H.; Oertel, D. C.; Bawendi, M. G. *J. Am. Chem. Soc.* **2006**, *128*, 13032. Joo, J.; Pietryga, J. M.; McGuire, J. A.; Jeon, S.-H.; Williams, D. J.; Wang, H.-L.; Klimov, V. I. *J. Am. Chem. Soc.* **2009**, *131*, 10620.
- (21) Biacchi, A. J.; Vaughn, D. D.; Schaak, R. E. *J. Am. Chem. Soc.* **2013**, *135*, 11634.
- (22) Moreels, I.; Lambert, K.; De Muynck, D.; Vanhaecke, F.; Poelman, D.; Martins, J. C.; Allan, G.; Hens, Z. *Chem. Mater.* **2007**, *19*, 6101.
- (23) Luther, J. M.; Jain, P. K.; Ewers, T.; Alivisatos, A. P. *Nat. Mater.* **2011**, *10*, 361.
- (24) Tsu, R.; Howard, W. E.; Esaki, L. *Phys. Rev.* **1968**, *172*, 779.